Greybody Factors of 2+1 Dimensional Charged Black Hole With Dilaton Field

Shakhawan Rafiq Hama Talib

Submitted to the
Institute of Graduate Studies and Research
in partial fulfillment of the requirements for the degree of

Master of Science
in
Physics

Eastern Mediterranean University
February 2016
Gazimağusa, North Cyprus

Approval of the Institute of Graduate Studies and Research

Prof. Dr. Cem Tanova
Acting Director

I certify that this thesis satisfies the requirements as a thesis for the degree of Master of Science in Physics.

Prof. Dr. Mustafa Halilsoy
Chair, Department of Physics

We certify that we have read this thesis and that in our opinion it is fully adequate in scope and quality as a thesis for the degree of Master of Science in Physics.

Assoc. Prof. Dr. İzzet Sakallı
Supervisor

Examining Committee

1. Prof. Dr. Mustafa Halilsoy

2. Assoc. Prof. Dr. S. Habib Mazharimousavi

3. Assoc. Prof. Dr. İzzet Sakallı

ABSTRACT

In this thesis, we analytically study the scalar perturbation of non-asymptotically flat 2+1 dimensional charged dilaton black holes. In particular, we show that radial wave equation is solved in terms of the hypergeometric functions. The analytical computations for the greybody factor, the absorption cross-section, and the decay rate for the massless scalar waves are elaborately made for these black holes. The results obtained for the aforementioned physical quantities are also plotted on the graphs.

Keywords: Black Hole, Greybody Factor, Absorption Cross-section, Decay Rate, Dilaton, Scalar Perturbation.

ÖZ

Bu tezde, asimptotoik olarak basık olmayan 2+1 boyutlu yüke ve dilatona sahip karadeliklerin skalar pertürbasyonunu çalışmaktayız. Özellikle, radyal dalga denkleminin hipergeometrik fonksiyonlar cinsinden çözülebildiğini göstermekteyiz. Bu karadelikler için gricisim faktörü, soğrulma enkesiti ve bozunma hızı analitik hesapları detaylı olarak yapılmıştır. Bahsi geçen fiziksel nicelikler için elde edilen sonuçların grafikleri de ayrıca çizilmiştir.

Anahtar Kelimeler: Karadelik, Gricisim Faktörü, Soğrulma Enkesiti, Bozunma Hızı, Dilaton, Skalar Pertürbasyon.

DEDICATION

This thesis is dedicated to:

- My beloved wife, Hawar, who has been a constant source of support and encouragement during my study and life.
- My lovely and caring daughter, Linda.
- All members of my family, especially to my: brother, Mohammed and my sister, Shayma.
- Dear my supervisor.

Shakhawan Rafiq Hama Talib

ACKNOWLEDGMENT

First of all I thank my God (Allah) for helping me to finalize this thesis.

I present my deepest appreciation to my supervisor Assoc. Prof. Dr. İzzet Sakallı because of his perfect supervision, informative advices, directives, and supportive encouragements. I will never forget his first sentence “if you continuously study to your project, you will never walk alone”.

I sincerely thank to my jury members Prof. Dr. Mustafa Halilsoy (Chairman), Assoc. Prof. Dr. S. Habib Mazharimousavi who participated to my defense. Their comments/suggestions helped me a lot to improve the thesis.

I would especially like to thank my family. I cannot find words to express how I am grateful to them for their endless love, support, and prays.

Finally, I would like to thank my best friends; in particular to Majeed J. Saleem for his continuous support and close interest.

TABLE OF CONTENTS

ABSTRACT iii

ÖZ iv

DEDICATION v

ACKNOWLEDGMENT vi

LIST OF FIGURES ix

1 INTRODUCTION 1

2 PHYSICAL PROPERTIES OF 3CDBH 3

3 SPIN-0 PERTURBATION OF 3CDBH 6

4 SOLUTION OF THE RADIAL EQUATION: COMPUTATION OF GBF, ACS AND DR 9

4.1 Near Horizon Solution 11

4.2 QNM of 3CDBH 11

4.3 GBF, ACS and DR Computation of 3CDBH 13

5 CONCLUSION 21

REFERENCES 22

LIST OF FIGURES

Figure 3.1: The plot of the potential $V(r)$ (3.7) versus r for ($\Lambda = 1, M = 10, Q = 1$ and $m = 0, 1$) 7

Figure 3.2: The plot of the potential $V(r)$ (3.7) versus r for ($\Lambda = 1, M = 10, Q = 1.25$ and $m = 0, 1$). Extermal case ($r_p = r_n$) 7

Figure 3.3: The plot of the potential $V(r)$ (3.7) versus r for ($\Lambda = 1, M = 10, Q = 0$ and $m = 0, 1$). Chargeless case ($r_n = 0$) 8

Figure 4.1: The plot of γ_{GbF} (4.50) versus ω for ($m = 0, 1$. 3CDBH configuration is set to $\Lambda = 1$, $M = 10$, and $Q = 1.245$) 15

Figure 4.2: The plot of γ_{GbF} (4.50) versus ω for ($m = 0, 1$. 3CDBH configuration is set to $\Lambda = 1.5$, $M = 10$, and $Q = 1$) 16

Figure 4.3: The plot of γ_{GbF} (4.50) versus ω for ($m = 0, 1$. 3CDBH configuration is set to $\Lambda = 0.5$, $M = 10$, and $Q = 1.2$) 16

Figure 4.4: The plot of σ_{abs} (4.56) versus ω for ($m = 0, 1$. 3CDBH configuration is set to $\Lambda = 1$, $M = 10$, and $Q = 1.245$) 18

Figure 4.5: The plot of σ_{abs} (4.56) versus ω for ($m = 0, 1$. 3CDBH configuration is set to $\Lambda = 1.5$, $M = 10$, and $Q = 1$) 18

Figure 4.6: The plot of σ_{abs} (4.56) versus ω for ($m = 0, 1$. 3CDBH configuration is set to $\Lambda = 0.5$, $M = 10$, and $Q = 1.2$) 19

Figure 4.7: The plot of Γ (4.58) versus ω for ($m = 0, 1$. 3CDBH configuration is set to $\Lambda = 1$, $M = 10$, and $Q = 1.245$) 19

Figure 4.8: The plot of Γ (4.58) versus ω for ($m = 0, 1$. 3CDBH configuration is set to $\Lambda = 1.5$, $M = 10$, and $Q = 1$) 20

Figure 4.9: The plot of Γ (4.58) versus ω for ($m = 0, 1$. 3CDBH configuration is set to $\Lambda = 0.5$, $M = 10$, and $Q = 1.2$)… 20

Chapter 1

INTRODUCTION

Hawking [1–2] showed that black holes (BHs) emit particles from their event horizon. This event is called as Hawking radiation (HR), which can be seen as a frontier station between general relativity (GR) and quantum mechanics (QM). From this aspect, it is also a key towards unlocking the mysteries of the quantum gravity theory (QGT).

Putting QGT into the process, BHs become no longer “black” but obey the laws of thermodynamics [3]. Namely, HR performs a characteristic blackbody radiation (CBR). However, this radiation still has to pass a non-trivial curved geometry before it reaches to an observer at spatial infinity. Namely, the surrounding spacetime thus manifests itself as a potential barrier for the HR, giving rise to a deviation from CBR spectrum as seen by the observer. The relative factor between the CBR and the asymptotic radiation spectrum is called the greybody factor (GbF). In other words, the gravitational potential enclosing the BH absorbs some of the radiation back into the BH and conveys the remaining to spatial infinity(SI), which results in a frequency dependent GbF.

Finding the GbFs leads someone to compute the absorption cross-section (ACS) and decay rate (DR) of the considered BH.

The studies on the GbFs go back to 1970s [4–8]. Since then the topic of the GbF has been intensively investigated by the researchers (see, for example, [9–11]). However, although there are many studies on the GbF for the asymptotically flat geometries (see, for instance, [12]), the number of studies regarding the non-asymptotically flat (NAF) BHs has remained limited.

The main purpose of this thesis is to study the propagation and dynamical evolution of the massless scalar fields, which obey the Klein-Gordon equation (KGE) in the 2+1 charged (NAF) dilaton BH (from now it will be referred as 3CDBH). Those BHs were derived by Chan and Mann [13]. In fact, my aim is to revisit the study of Fernando [14], who first analyzed the GbF, ACS, and DR of the 3CDBH. To this end, I shall show that the Fernando's results could be obtained with anew solution to the KGE in the geometry of 3CDBH.

The thesis is organized as follows. Chapter 2 introduces 3CDBH spacetime. Analysis of the KGE in this geometry is given in Chapter 3. Chapter 4 is devoted to the radial solution. In sequel. Quasinormal mode (QNM), GbF, ACS, and DR computations are considered for 3CDBH. The thesis ends with a conclusion in Chapter 5.

Chapter 2

PHYSICAL PROPERTIES OF 3CDBH

In this chapter I will represent the geometrical and thermodynamical features of the 3CDBH. The solution of the 3CDBH was found by Chan and Mann [13].

In this context, let us first consider the Einstein-Maxwell-Dilaton Λ action (in respect there of the low-energy string action), which is given by

$$I = \int d^3x\sqrt{-g}\left(\mathcal{R} + 2e^{ь\varphi}\Lambda - \frac{\mathcal{B}}{2}(\nabla\varphi)^2 - e^{-4ą\varphi}F_{\mu\nu}F^{\mu\nu}\right), \tag{2.1}$$

where $F_{\mu\nu}$ is the Maxwell tensor, φ denotes the dilaton field, $\mathcal{B}, ą$, and ь are free constants, and $\mathcal{R}$ stands for the Ricci scalar in three dimensions. Λ-symbol represents the cosmological constant such that while positive Λ's describe the anti-de Sitter (AdS) spacetime, negative Λ's manifest the de Sitter (dS) spacetime.

The resulting metric solution, which is static and circularly symmetric is given by [13]

$$ds^2 = -f(r)dt^2 + 4\frac{r^{\frac{4}{N}-2}}{N^2\tilde{\gamma}^{\frac{4}{N}}}f(r)^{-1}dr^2 + r^2d\theta^2, \tag{2.2}$$

by which the metric function:

$$f(r) = -\mathcal{A}r^{\frac{2}{3}-1} + \frac{8\Lambda r^2}{(3N-2)N} + \frac{8Q^2}{(2-N)N}. \tag{2.3}$$

It is obvious that the geometry (2.2) exhibits a NAF structure. Therefore it can not behave asymptotically as dS or AdS [13]. In fact, the latter remark is due to the non-trivial dilaton field φ. The dilaton and the non-zero Maxwell tensor are given by

$$\varphi = \frac{2\tilde{\kappa}}{N} ln\left[\frac{r}{\beta(\tilde{\gamma})}\right]. \tag{2.4}$$

$$F_{tr} = \frac{2}{N}\tilde{\gamma}^{-\frac{2}{N}} r^{\frac{2}{N}} Q e^{4ąφ}, \tag{2.5}$$

where $\beta, \tilde{\gamma}$ are constants, N denotes the Lagrange multiplier that imposes a constant on the action, and Q is the electric charge. On the other hand, $\tilde{\kappa}$ is another constant given by

$$\tilde{\kappa} = \pm\sqrt{\frac{N}{\mathcal{B}}\left(1 - \frac{N}{2}\right)}\ . \tag{2.6}$$

$$4ą\tilde{\kappa} = ь\tilde{\kappa} = N - 2\ . \tag{2.7}$$

$$4ą = ь. \tag{2.8}$$

As it was stated in the paper [13], when $(\Lambda, \mathcal{B}) > 0$ and $2 > N > \frac{2}{3}$, the solution (2.2) with anew metric function (2.3) represents a BH. Hence, the constant $\mathcal{A}$ gains a physical property: the quasi-local mass M [15]. This mass could be estimated via the Brown-York formalism [15] as follows

$$M = -\frac{N_{\circ}\mathcal{A}}{2}. \tag{2.9}$$

It is clear from Eq. (2.9) that having $M > 0$, one should consider negative $\mathcal{A}$ values. As seen in [14], throughout this paper I restrict my attention to the BHs configured with $N = \tilde{\gamma} = \beta = ą = \frac{ь}{4} = \frac{\mathcal{B}}{8} = -4\tilde{\kappa} = 1$. These choices modify the physical quantities to

$$f(r) = -2Mr + 8\Lambda r^2 + 8Q^2\ . \tag{2.10}$$

$$\varphi = -\frac{1}{2} ln(r). \tag{2.11}$$

$$F_{tr} = \frac{2Q}{r^2}. \tag{2.12}$$

From Eq. (2.10) (after getting its roots), one can understand that $M \geq 8Q\sqrt{\Lambda}$ for the BH solutions. Thus , the two horizons (coordinate singularities) of the BH read

$$r_p = M\frac{1+E}{8\Lambda}, \qquad r_n = M\frac{1-E}{8\Lambda}, \tag{2.13}$$

where

$$E = \sqrt{1-\frac{64Q^2\Lambda}{M^2}} = \frac{4\Lambda}{M}\left(r_p - r_n\right), \quad (0 < E < 1). \tag{2.14}$$

In Eq. (2.13) r_p and r_n are called the outer and inner horizons of the 3CDBH, respectively. Thus, the metric function can be rewritten as

$$f(r) = 8\Lambda(r - r_p)(r - r_n). \tag{2.15}$$

It is needless to say that the physical singularity is at $r = 0$. The 3CDBHs can perform a Hawking radiation with the Hawking temperature (T_H) [16]:

$$T_H = \frac{\kappa}{2\pi} = \frac{|g'_{tt}|}{4\pi}\sqrt{-g^{tt}g^{rr}}\Big|_{r=r_p} = \frac{M}{4\pi r_p}E = \frac{\Lambda}{\pi r_p}\left(r_p - r_n\right). \tag{2.16}$$

In the above equation, κ denotes the surface gravity, which is equal to

$$\kappa = \frac{2\Lambda}{r_p}(r_p - r_n). \tag{2.17}$$

(Note that throughout the thesis, a prime over a quantity denotes derivative with respect to its argument).

Chapter 3

SPIN-0 PERTURBATION OF 3CDBH

In this chapter we will study the KGE in the background of 3CDBH. The general equation for a massless scalar field in the curved spacetime is given by,

$$\nabla^2\Phi = 0, \tag{3.1}$$

that corresponds to

$$\frac{1}{\sqrt{-g}}\partial_\mu\left(\sqrt{-g}g^{\mu v}\partial_v\Phi\right) = 0. \tag{3.2}$$

Applying the ansatz,

$$\Phi = e^{-i\omega t}e^{im\theta}R(r). \tag{3.3}$$

In Eq. (3.2) admits the following radial equation,

$$\frac{d}{dr}\left(f(r)\frac{dR(r)}{dr}\right) + 4r^2\left(\frac{\omega^2}{f(r)} - \frac{m^2}{r^2}\right)R(r) = 0, \tag{3.4}$$

which can be recast into the Schrödinger like wave equation,

$$\left(\frac{d^2}{dr_*^2} + \omega^2 - V(r)\right)R(r) = 0. \tag{3.5}$$

Here, r_* is the tortoise coordinate:

$$r_* = \int\frac{2rdr}{f}, \tag{3.6}$$

and the potential $V(r)$ reads

$$V(r) = 8m^2\Lambda + 4\Lambda^2 - \frac{2m^2M}{r} + \frac{8m^2Q^2 - 8\Lambda Q^2 - \frac{M^2}{4}}{r^2} + \frac{4MQ^2}{r^3} - \frac{12Q^4}{r^4}. \tag{3.7}$$

The plots of the potential $V(r)$ versus r are depicted in Figures (3.1-3.3).

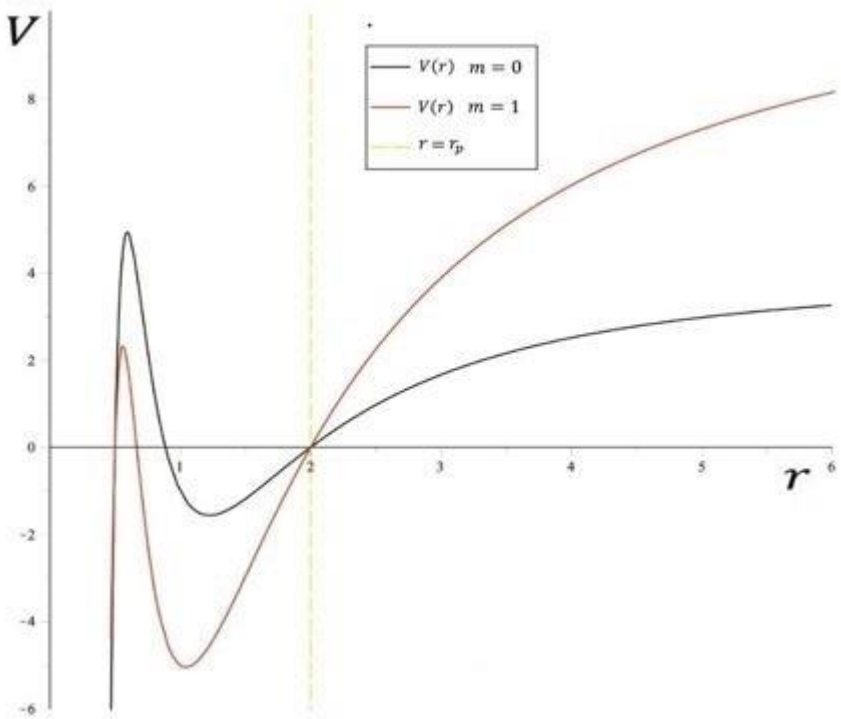

Figure 3.1: The behaviors of $V(r)$ for $M = 10$, $\Lambda = 1$, $Q = 1$, and $m = 0, 1$.

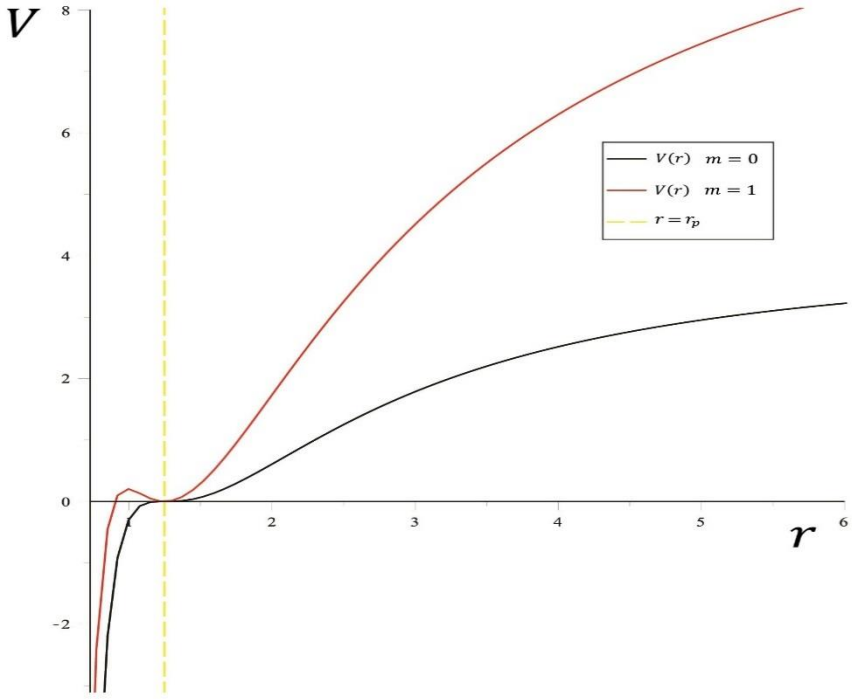

Figure 3.2: The behaviors of $V(r)$ for $M = 10$, $\Lambda = 1$, $Q = 1.25$, and $m = 0, 1$: Extremal case ($r_p = r_n$).

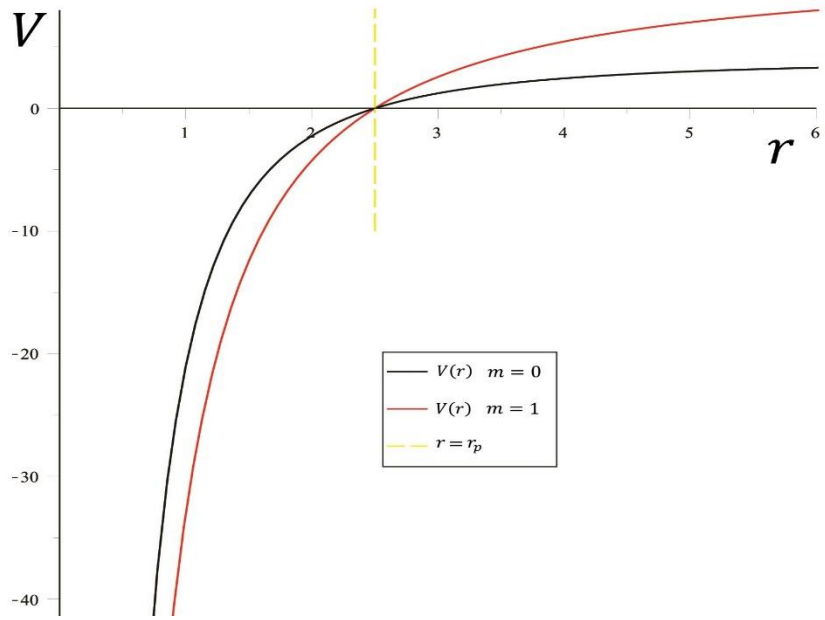

Figure 3.3: The behaviors of $V(r)$ for $M = 10$, $\Lambda = 1$, $Q = 0$, and $m = 0, 1$: Chargeless case ($r_n = 0$).

Chapter 4

SOLUTION OF THE RADIAL EQUATION: COMPUTATION OF GbF, ACS, AND DR

In this chapter, I will present the analytical solution of the radial equation. To this end, I introduce a new variable z as follows,

$$z = \frac{r-r_p}{r_p-r_n}. \tag{4.1}$$

Thus, the radial equation (3.4) becomes

$$4\Lambda z(1+z)\frac{d^2R(z)}{dz^2} + 4\Lambda(1+2z)\frac{dR(z)}{dz} + G1(z)R(z) = 0, \tag{4.2}$$

where

$$G1(z) = \frac{A^2}{z} + \frac{B^2}{z+1} + C, \tag{4.3}$$

in which

$$A = \frac{r_p\omega}{2\sqrt{\Lambda}(r_p-r_n)} = \frac{\omega\sqrt{\Lambda}}{\kappa}, \tag{4.4}$$

$$B = \frac{i\omega r_n}{2\sqrt{\Lambda}(r_n-r_p)}, \tag{4.5}$$

$$C = \frac{\omega^2-8m^2\Lambda}{4\Lambda}. \tag{4.6}$$

Letting

$$R(z) = z^{i\alpha}(1+z)^{-\beta}F(z), \tag{4.7}$$

where

$$\alpha = \frac{A}{2\sqrt{\Lambda}} = \frac{\omega}{2\kappa}, \tag{4.8}$$

$$\beta = \frac{B}{2\sqrt{\Lambda}} = \frac{i\omega r_n}{4\Lambda(r_n - r_p)}, \tag{4.9}$$

the solution of the radial equation (4.2) now reads

$$R(z) = C_1 z^{i\alpha}(1+z)^{-\beta}F(a,b,c,-z) + C_2 z^{-i\alpha}(1+z)^{-\beta}F(\tilde{a},\tilde{b},\tilde{c},-z), \tag{4.10}$$

where $F(a,b;c;-z)$ is the hypergeometric function [17] and C_1, C_2 are the integration constants. The functional parameters $\tilde{a}$, $\tilde{b}$ and $\tilde{c}$ are given by

$$\begin{aligned} \tilde{a} &= a - c + 1, \\ \tilde{b} &= b - c + 1, \\ \tilde{c} &= 2 - c, \end{aligned} \tag{4.11}$$

where

$$a = \frac{1}{2} + \frac{iA-B}{2\sqrt{\Lambda}} + \frac{1}{2}\sqrt{\frac{C}{\Lambda} - 1}, \tag{4.12}$$

$$b = \frac{1}{2} + \frac{iA-B}{2\sqrt{\Lambda}} - \frac{1}{2}\sqrt{\frac{C}{\Lambda} - 1}, \tag{4.13}$$

$$c = 1 + \frac{iA}{\sqrt{\Lambda}}. \tag{4.14}$$

In the line of the work of Fernando [14], in this thesis I will consider only the perturbations with large frequencies. Namely, I will assume that

$$\frac{C}{\Lambda} \geq 1, \quad \Rightarrow \quad \xi^2 = \frac{\omega^2 - 8m^2\Lambda}{4\Lambda^2} \geq 1, \tag{4.15}$$

$$\gamma = \frac{1}{2}\sqrt{\frac{C-\Lambda}{\Lambda}} = \frac{1}{4\Lambda}\sqrt{\omega^2 - 8m^2\Lambda - 4\Lambda^2}, \tag{4.16}$$

$$\gamma = \frac{1}{2}\sqrt{\frac{\omega^2 - 8m^2\Lambda}{4\Lambda^2} - 1} = \frac{1}{2}\sqrt{\xi^2 - 1}\,. \tag{4.17}$$

4.1 Near Horizon Solution

In the vicinity of the horizon ($z \to 0$), the hypergeometric functions seen in the solution (4.10) become

$$F(a, b; c; -z) \to 1, \tag{4.18}$$

and the analytic function $R(z)$ behaves as

$$R(z) = C_1(z)^{i\alpha} + C_2(z)^{-i\alpha}. \tag{4.19}$$

If we expand the metric function (2.15) into series via the Taylor series with respect to r around the event horizon r_p:

$$f(r) \simeq f'(r_p)(r - r_p) + O(r - r_p)^2, \tag{4.20}$$

$$\simeq 4r_p\kappa(r - r_p). \tag{4.21}$$

Now the tortoise coordinate (3.6) modifies to

$$r_* \simeq \frac{1}{2\kappa} ln(z), \tag{4.22}$$

or equivalently

$$z \simeq e^{2\kappa r_*}. \tag{4.23}$$

Whence near horizon waves are governed by

$$\Phi \simeq C_1 e^{-i\omega(t-r_*)} + C_2 e^{-i\omega(t+r_*)}. \tag{4.24}$$

From Eq. (4.24), I understand that while the first term corresponds to an outgoing wave, the second one is an ingoing wave [18].

4.2 QNM of 3CDBH

For the computation of QNMs, one has to impose the boundary condition, which requires the pure ingoing wave at the horizon. This can be achieved by simply setting

$C_1 = 0$ in the general solution (4.10). Thus, we have

$$R(z) = C_2 z^{-i\alpha}(1+z)^{-\beta} F(\tilde{a}, \tilde{b}, \tilde{c}, -z). \tag{4.25}$$

To overlap the near-horizon and asymptotic regions, now I am interested with the large behavior ($r \simeq r_* \simeq z \simeq 1 + z \to \infty$) of the solution (4.24). For this purpose, I use the following the transformation formula [19].

$$F\left(\tilde{a}, \tilde{b}, \tilde{c}; x\right) = \frac{\Gamma(\tilde{c})\Gamma(\tilde{b}-\tilde{a})}{\Gamma(\tilde{b})\Gamma(\tilde{c}-\tilde{a})}(-x)^{-\tilde{a}} F\left(\tilde{a}, \tilde{a}+1-\tilde{c}; \tilde{a}+1-\tilde{b}; \frac{1}{x}\right) +$$

$$\frac{\Gamma(\tilde{c})\Gamma(\tilde{a}-\tilde{b})}{\Gamma(\tilde{a})\Gamma(\tilde{c}-\tilde{b})}(-x)^{-\tilde{b}} F\left(\tilde{b}, \tilde{b}+1-\tilde{c}; \tilde{b}+1-\tilde{a}; \frac{1}{x}\right). \tag{4.26}$$

So, one obtains the asymptotic behavior of the radial solution (4.24) as

$$R(r) \approx \frac{C_2}{\sqrt{r}}\left[\frac{\Gamma(\tilde{c})\Gamma(\tilde{b}-\tilde{a})}{\Gamma(\tilde{b})\Gamma(\tilde{c}-\tilde{a})}(r)^{-i\gamma} + \frac{\Gamma(\tilde{c})\Gamma(\tilde{a}-\tilde{b})}{\Gamma(\tilde{a})\Gamma(\tilde{c}-\tilde{b})}(r)^{i\gamma}\right]. \tag{4.27}$$

Meanwhile, since the metric function (2.15) around spatial infinity approximates to

$$f_{SI} \simeq 8\Lambda r^2, \tag{4.28}$$

and the tortoise coordinate at spatial infinity reads

$$r_* \simeq \int \frac{2rdr}{f_{SI}} = \int \frac{2rdr}{8\Lambda r^2} = \frac{1}{4\Lambda} lnr, \tag{4.29}$$

which is equivalent to

$$r \simeq e^{4\Lambda r_*}. \tag{4.30}$$

Thus, the first and second terms in the square bracket of Eq. (4.27) are interpreted as ingoing and outgoing asymptotic waves, respectively. The other boundary condition of the QNM imposes that the ingoing waves spontaneously vanish at spatial infinity. In other words, only purely outgoing waves are allowed to survive at spatial infinity.

Mathematically speaking, the first term of Eq. (4.27) must be zero. This is possible by the poles of the Gamma function [17] in the denominator of the second term; $\Gamma(c-a)$ or $\Gamma(b)$. As the Gamma function $\Gamma(p)$ possesses the poles at $p=-n$ for $n=0,1,2,\ldots$, the wave function fulfills the associated boundary condition with the following provisions:

$$\tilde{c}-\tilde{a}=1-\tilde{a}=-n. \tag{4.31}$$

From Eqs. (4.28) and (4.29), one can determine the first set of QNMs of 3CDBH as

$$\omega_1=\frac{-2I(-2\Lambda n(n+1)+m^2)}{1+2n}. \tag{4.32}$$

It is worth noting that QNMs should perform damping if and only if

$$m^2\geq 2\Lambda n(n+1). \tag{4.33}$$

The second set of QNMs are determined by

$$\tilde{b}=-n, \tag{4.34}$$

which yields

$$\omega_2=\frac{-2I(2\Lambda n(n+1)-m^2)}{1+2n}. \tag{4.35}$$

It is worth noting that QNMs should perform damping if and only if

$$m^2\leq 2\Lambda n(n+1). \tag{4.36}$$

4.3 GbF, ACS and DR Computations of 3CDBH

GbF is generally determined by the flux of the wave propagating from the horizon to the asymptotic infinity. The conserved flux for the wave function is given by [20].

$$\mathcal{F}=\frac{2\pi}{i}\left[R^*(r)f(r)\frac{dR(r)}{dr}-R(r)f(r)\frac{dR^*}{dr}\right], \tag{4.37}$$

where * over a quantity denotes the complex conjugation. Using Eq. (4.25), the ingoing flux for the horizon reads

$$\mathcal{F}\left(r \to r_p\right) = -8\pi\omega|C_2|^2 r_p. \tag{4.38}$$

Using Eq. (4.27) for the function $R(r)$ at spatial infinity, the incoming flux at spatial infinity is given by,

$$\mathcal{F}(r \to \infty) = -32\pi\Lambda|D_2|^2\gamma(r_p - r_n), \tag{4.39}$$

where

$$D_2 = \frac{\Gamma(\tilde{c})\Gamma(\tilde{b}-\tilde{a})}{\Gamma(\tilde{b})\Gamma(\tilde{c}-\tilde{a})} C_2. \tag{4.40}$$

The partial wave absorption or the greybody factor [21] is given by

$$\gamma_{GbF} = \frac{\mathcal{F}\left(r \to r_p\right)}{\mathcal{F}(r \to \infty)}. \tag{4.41}$$

By inserting the values of α and β into the above expression, and in sequel by using the following identities:

$$\left|\Gamma\left(\frac{1}{2} + i\xi\right)\right|^2 = \frac{\pi}{cosh(\pi\xi)}, \tag{4.42}$$

$$|\Gamma(i\xi)|^2 = \frac{\pi}{\xi sinh(\pi\xi)}, \tag{4.43}$$

$$|\Gamma(1 + i\xi)|^2 = \frac{\pi\xi}{sinh(\pi\xi)}. \tag{4.44}$$

Eq. (4.41) transforms into

$$\gamma_{GbF} = \frac{sinh(\pi y_0)\, sinh(\pi y_3)}{cosh(\pi y_1)\, cosh(\pi y_2)}, \tag{4.45}$$

where

$$y_0 = -\frac{\omega}{\kappa}, \tag{4.46}$$

$$y_1 = \frac{\omega}{2\kappa}\left(\frac{r_n - r_p}{r_p}\right) - \gamma, \tag{4.47}$$

$$y_2 = -2\gamma, \tag{4.48}$$

$$y_3 = -\frac{\omega}{2\kappa}\left(\frac{r_p + r_n}{r_n}\right) - \gamma, \tag{4.49}$$

$$\gamma_{GbF} = \frac{sinh\left(\frac{\pi\omega}{\kappa}\right) sinh\left(\frac{\pi\omega}{2\kappa}\left(\frac{r_p + r_n}{r_n}\right) + \pi\gamma\right)}{cosh\left(\frac{\pi\omega}{2\kappa}\left(\frac{r_n - r_p}{r_p}\right) - \pi\gamma\right) cosh(-2\pi\gamma)}. \tag{4.50}$$

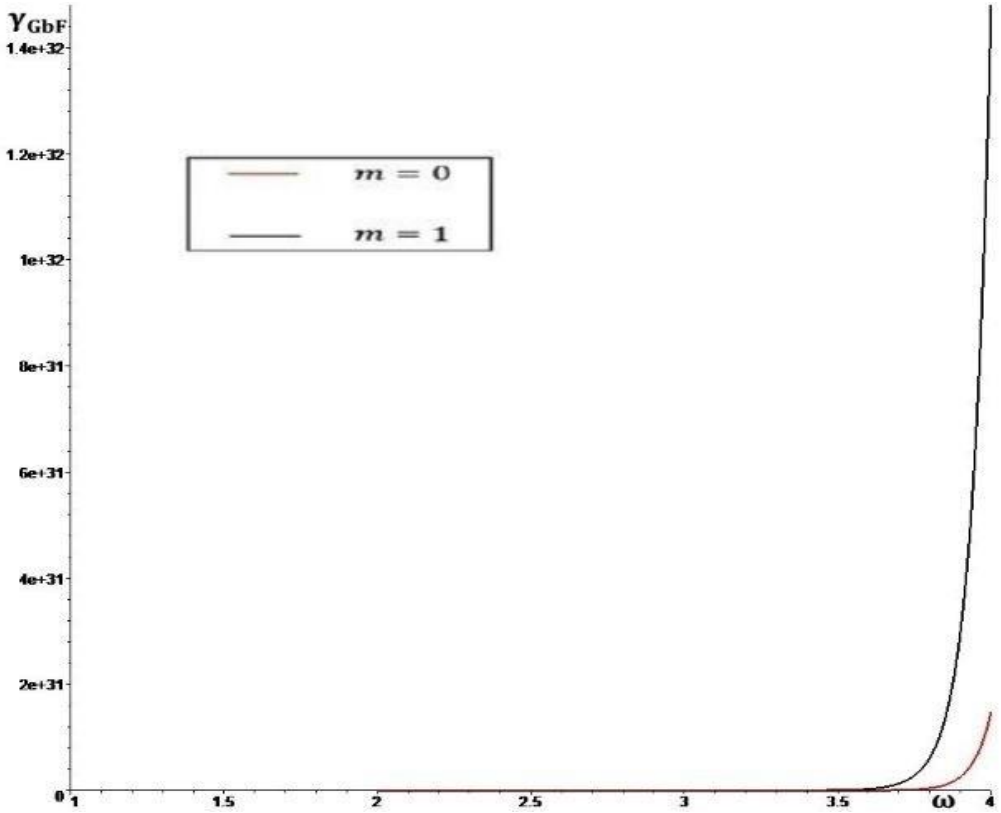

Figure 4.1: The plot of γ_{GbF} (4.50) versus ω for $m = 0, 1$. 3CDBH configuration is set to $\Lambda = 1$, $M = 10$, and $Q = 1.245$.

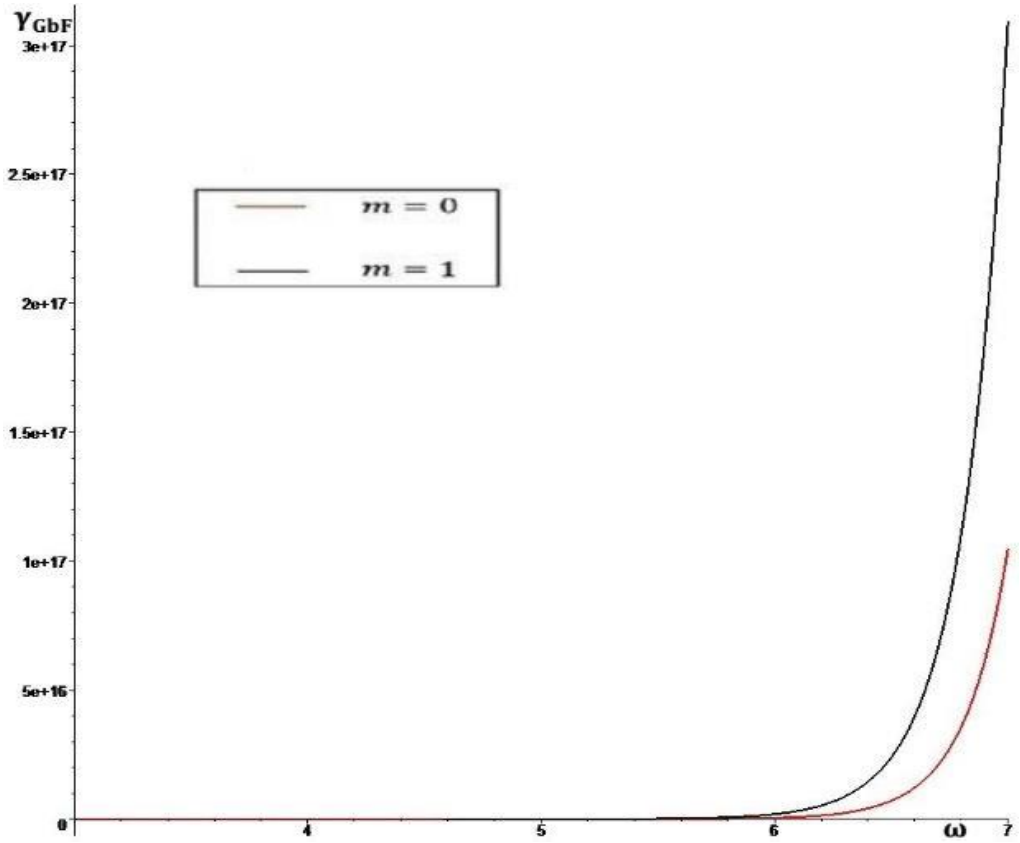

Figure 4.2: The plot of γ_{GbF} (4.50) versus ω for $m = 0, 1$. 3CDBH configuration is set to $\Lambda = 1.5$, $M = 10$, and $Q = 1$.

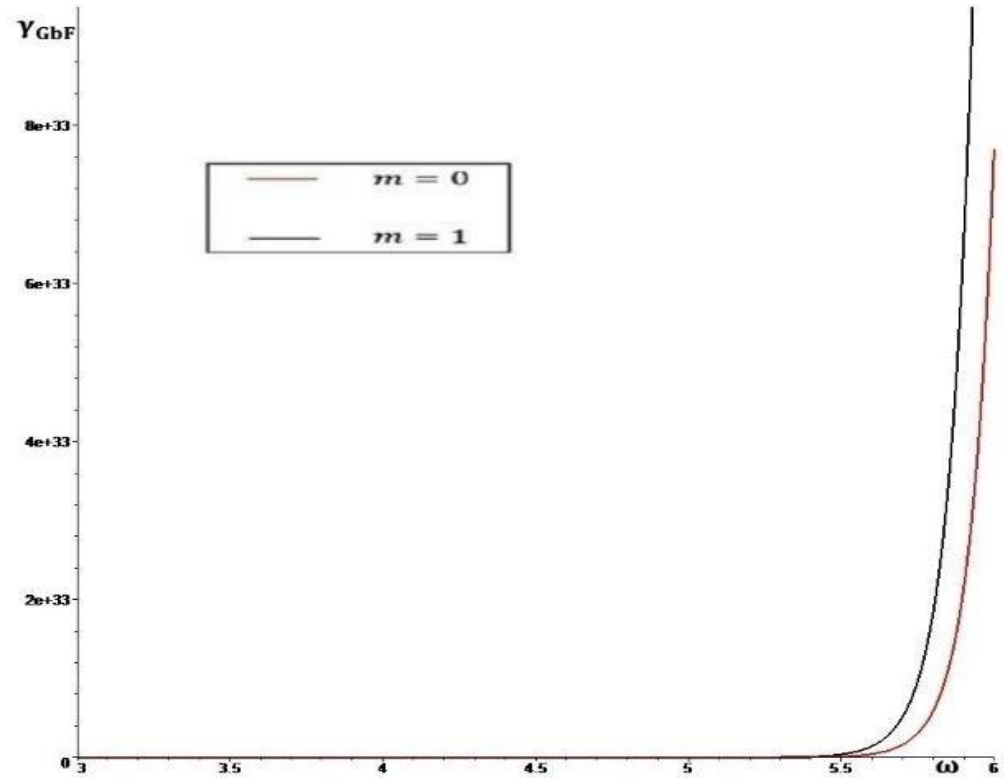

Figure 4.3: The plot of γ_{GbF} (4.50) versus ω for $m = 0, 1$. 3CDBH configuration is set to $\Lambda = 0.5$, $M = 10$, and $Q = 1.2$

The ACS in three dimensions is given by [22] as follows

$$\sigma_{abs} = \frac{\gamma_{GbF}}{\omega}. \tag{4.51}$$

So the exponential form of the ACS becomes

$$\sigma_{abs} = \frac{\gamma_{GbF}}{\omega} = \frac{1}{\omega}\frac{(e^{\pi y_0} - e^{-\pi y_0})(e^{\pi y_3} - e^{-\pi y_3})}{(e^{\pi y_1} + e^{-\pi y_1})(e^{\pi y_2} + e^{-\pi y_2})}, \tag{4.52}$$

$$= \frac{1}{\omega}\frac{\left(e^{-\frac{\pi\omega}{\kappa}} - e^{\frac{\pi\omega}{\kappa}}\right)\left(e^{-\frac{\pi\omega}{2\kappa}(\frac{r_p+r_n}{r_n})-\pi\gamma} - e^{\frac{\pi\omega}{2\kappa}(\frac{r_p+r_n}{r_n})+\pi\gamma}\right)}{\left(e^{\frac{\pi\omega}{2\kappa}(\frac{r_n-r_p}{r_p})-\pi\gamma} + e^{-\frac{\pi\omega}{2\kappa}(\frac{r_n-r_p}{r_p})+\pi\gamma}\right)(e^{-2\pi\gamma} + e^{2\pi\gamma})}, \tag{4.53}$$

$$= \frac{1}{\omega}\frac{e^{-\frac{\pi\omega}{\kappa}}\left(e^{\frac{2\pi\omega}{\kappa}} - 1\right)\left(e^{\frac{\pi\omega}{2\kappa}(\frac{r_p+r_n}{r_n})+\pi\gamma} - e^{-\frac{\pi\omega}{2\kappa}(\frac{r_p+r_n}{r_n})-\pi\gamma}\right)}{\left(e^{\frac{\pi\omega}{2\kappa}(\frac{r_n-r_p}{r_p})-\pi\gamma} + e^{-\frac{\pi\omega}{2\kappa}(\frac{r_n-r_p}{r_p})+\pi\gamma}\right)(e^{-2\pi\gamma} + e^{2\pi\gamma})}. \tag{4.54}$$

Recalling

$$T_H = \frac{\kappa}{2\pi} \Rightarrow \frac{1}{T_H} = \frac{2\pi}{\kappa}, \tag{4.55}$$

we finally get

$$\sigma_{abs} = \frac{1}{\omega}\frac{e^{-\frac{\pi\omega}{\kappa}}\left(e^{\frac{\omega}{T_H}} - 1\right)\left(e^{\frac{\pi\omega}{2\kappa}(\frac{r_p+r_n}{r_n})+\pi\gamma} - e^{-\frac{\pi\omega}{2\kappa}(\frac{r_p+r_n}{r_n})-\pi\gamma}\right)}{\left(e^{\frac{\pi\omega}{2\kappa}(\frac{r_n-r_p}{r_p})-\pi\gamma} + e^{-\frac{\pi\omega}{2\kappa}(\frac{r_n-r_p}{r_p})+\pi\gamma}\right)(e^{-2\pi\gamma} + e^{2\pi\gamma})}. \tag{4.56}$$

The DR expression for a BH is given by [20]

$$\Gamma = \frac{\sigma_{abs}}{\frac{\omega}{e^{T_H}} - 1}, \tag{4.57}$$

where T_H denotes the temperature for the 3CDBH seen in Eq. (2.16). Hence DR simplifies to

$$\Gamma = \frac{1}{\omega}\frac{e^{-\frac{\pi\omega}{\kappa}}\left(e^{\frac{\pi\omega}{2\kappa}(\frac{r_p+r_n}{r_n})+\pi\gamma} - e^{-\frac{\pi\omega}{2\kappa}(\frac{r_p+r_n}{r_n})-\pi\gamma}\right)}{\left(e^{\frac{\pi\omega}{2\kappa}(\frac{r_n-r_p}{r_p})-\pi\gamma} + e^{-\frac{\pi\omega}{2\kappa}(\frac{r_n-r_p}{r_p})+\pi\gamma}\right)(e^{-2\pi\gamma} + e^{2\pi\gamma})}. \tag{4.58}$$

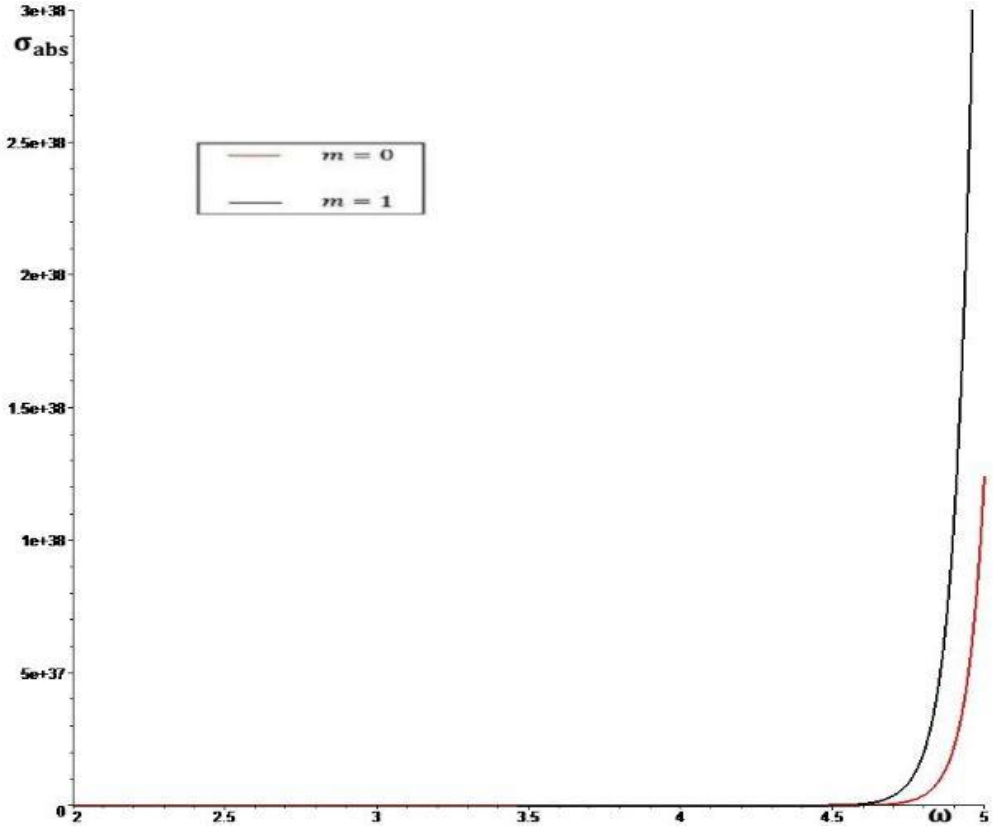

Figure 4.4: The plot of σ_{abs} (4.56) versus ω for $m = 0, 1$. 3CDBH configuration is set to $\Lambda = 1$, $M = 10$, and $Q = 1.245$.

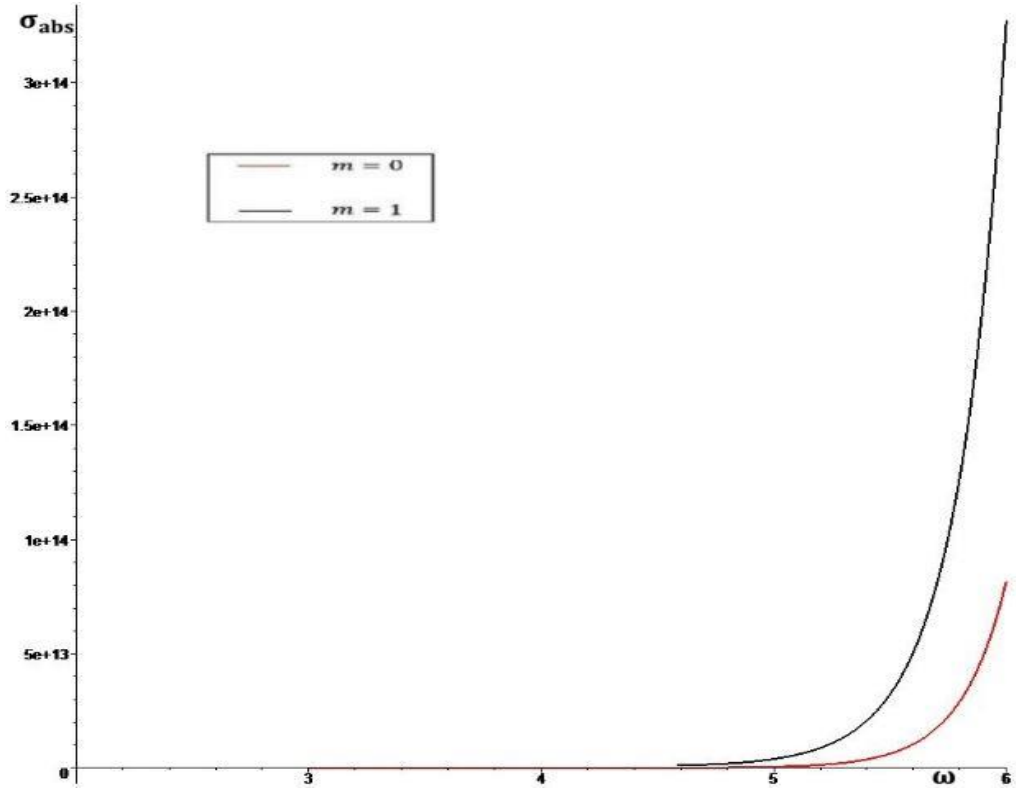

Figure 4.5: The plot of σ_{abs} (4.56) versus ω for $m = 0, 1$. 3CDBH configuration is set to $\Lambda = 1.5$, $M = 10$, and $Q = 1$.

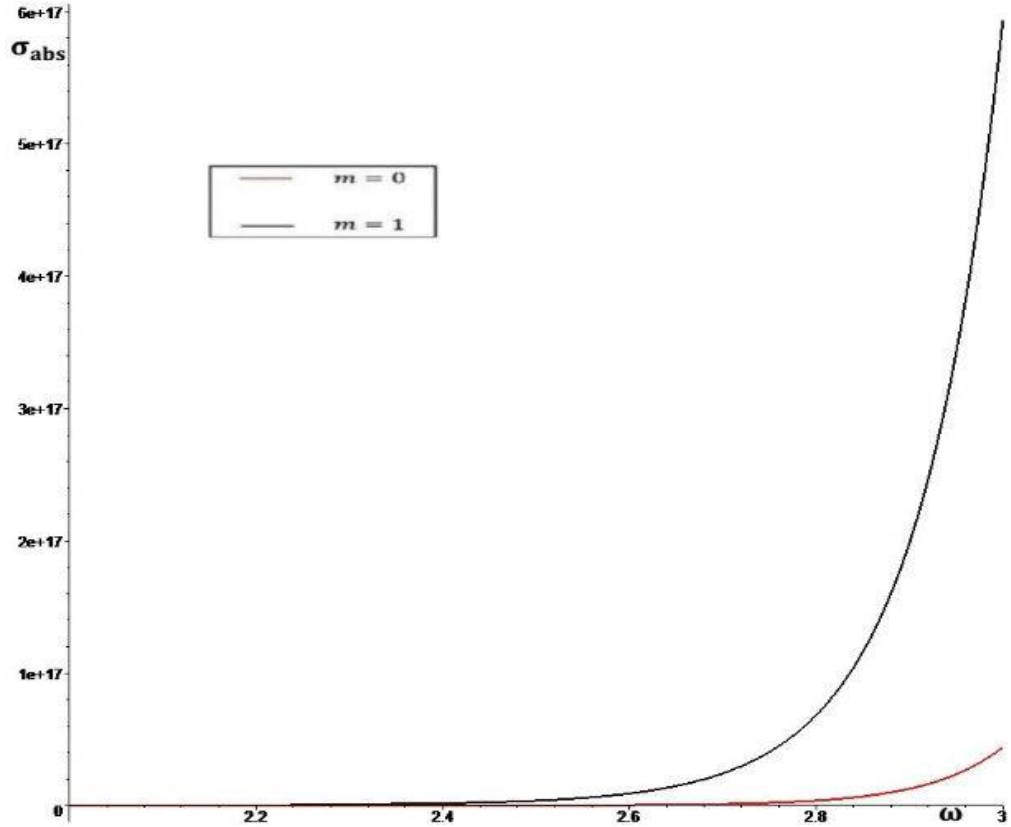

Figure 4.6: The plot of σ_{abs} (4.56) versus ω for $m = 0, 1$. 3CDBH configuration is set to $\Lambda = 0.5$, $M = 10$, and $Q = 1.2$.

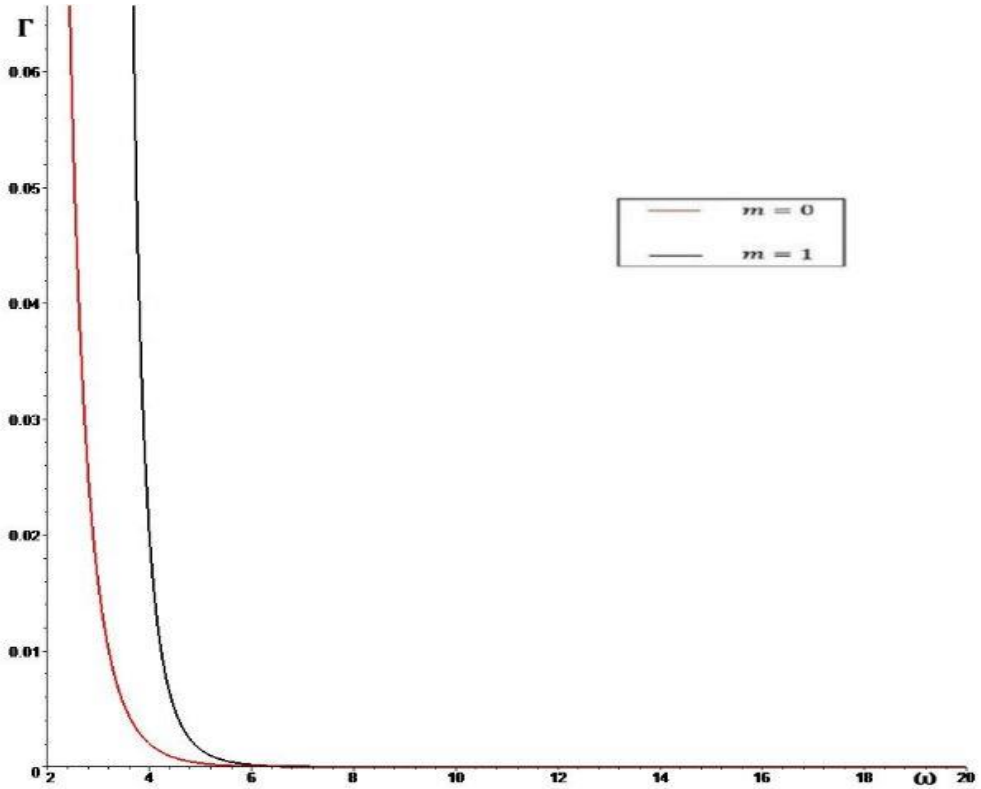

Figure 4.7: The plot of Γ (4.58) versus ω for $m = 0, 1$. 3CDBH configuration is set to $\Lambda = 1$, $M = 10$, and $Q = 1.245$.

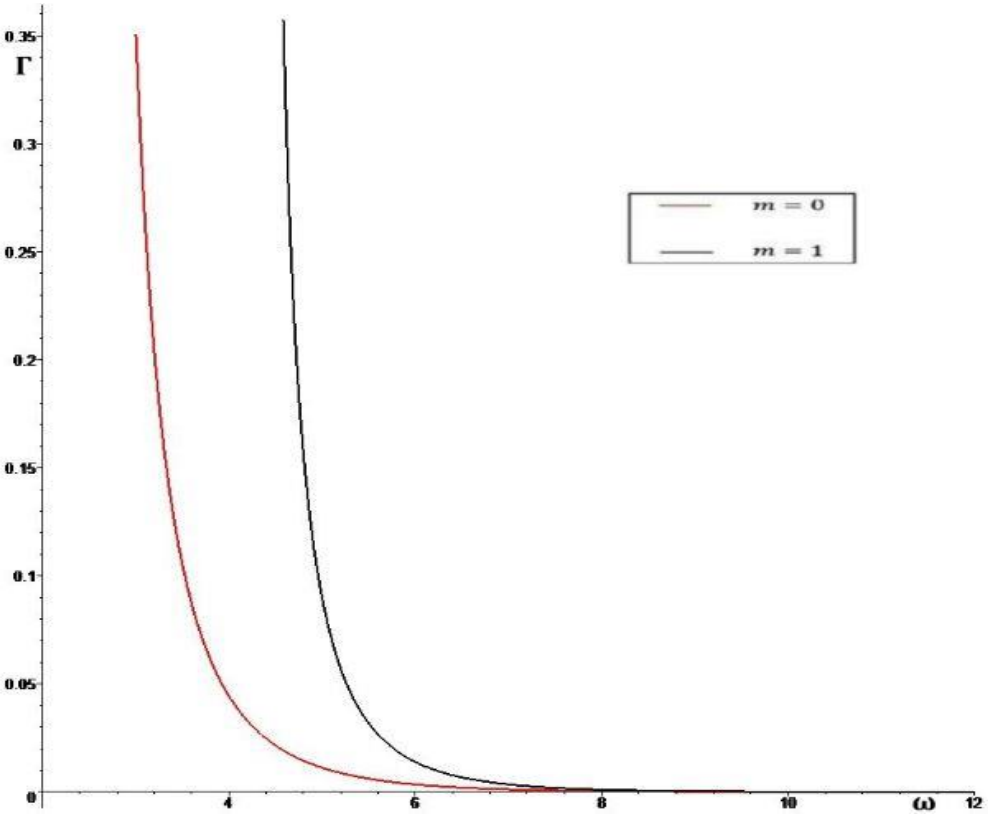

Figure 4.8: The plot of Γ (4.58) versus ω for $m = 0, 1$. 3CDBH configuration is set to $\Lambda = 1.5$, $M = 10$, and $Q = 1$.

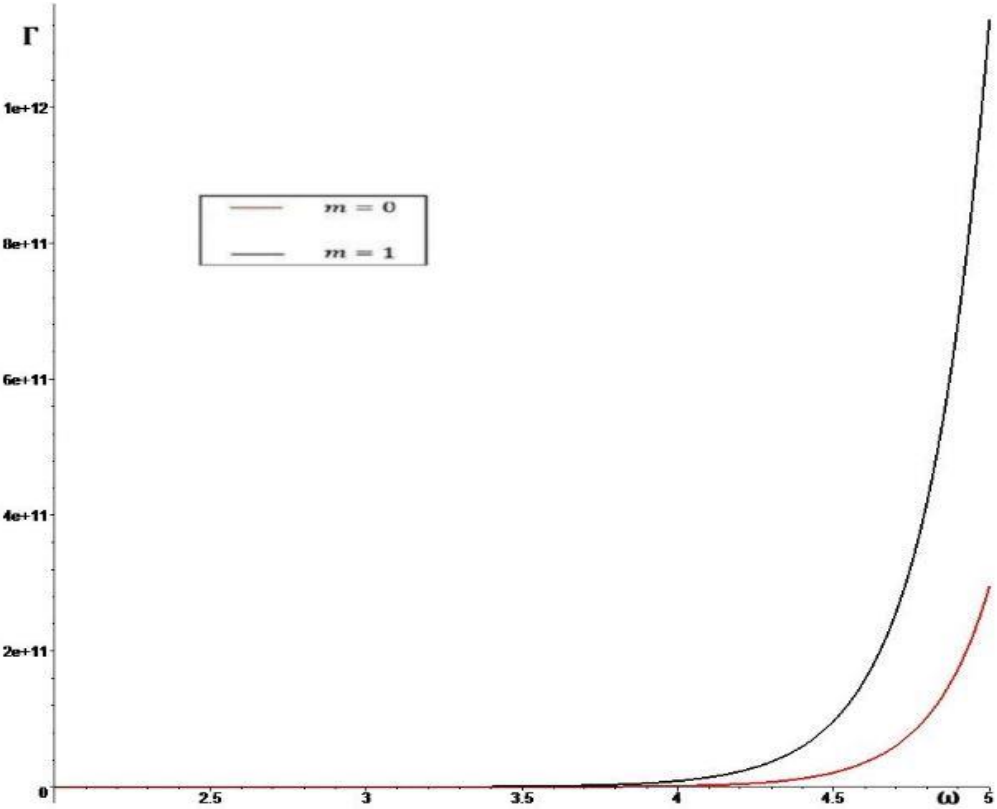

Figure 4.9: The plot of Γ (4.58) versus ω for $m = 0, 1$. 3CDBH configuration is set to $\Lambda = 0.5$, $M = 10$, and $Q = 1.2$.

Chapter 5

CONCLUSION

I have thoroughly studied the propagation of the massless scalar fields in the background of the 3CDBH. I have obtained an analytical solution for the KGE in the 3CDBH background. Then, taking the recognizance the appropriate boundary conditions, I have obtained an exact expression for the GbF of the scalar fields moving in the 3CDBH geometry. Subsequently, I have computed the analytical ACS and DR for the 3CDBH s. In Figs. (4.1-4.3), (4.4-4.6) and (4.7-4.9), I have shown the behaviors of GbF, ACS, and DR with varying frequencies that satisfy the condition (4.15). Furthermore, for the lower frequencies ($0 \leq \frac{\omega^2-8m^2\Lambda}{4\Lambda} < 1$) I have understood that the incoming flux (4.39) vanishes at SI (similar to [14]), which leads to diverging GbF. This problem could be fixed by the procedure described in [12]. However, this aspect was out of the scope of the present thesis.

Finally, I would like to state that my future plan is to extend my analyses to the 4-dimensional (even to higher dimensions, $N \geq 5$) BH geometries [23].

REFERENCES

[1] Hawking, S. W. (1975). Particle creation by black holes. *Commun. Math. Phys.* 43, 199-220.

[2] Hawking, S. W. (1976). Particle creation by black holes. *Commun. Math. Phys.* 46, 206.

[3] Bardeen, J. M., Carter, B., & Hawking, S. W. (1973). The four laws of black hole mechanics. *Commun. Math. Phys*. 31, 161.

[4] Strobinskii, A. A. (1973). Amplification of wave during reflection from a rotation black hole. *Zh. Eksp. Teor. Fiz.* 64, 48-57.

[5] Starobinskii, A. A., & Churilov, S. M. (1973). Amplification of electromagnetic and gravitational waves scattered by a rotating black hole. *Zh. Eksp. Teor. Fiz.* 65, 3-11.

[6] Page, D. N. (1976). Particle emission rates from a black hole: Massless particles from an uncharged, nonrotating hole. *Phys. Rev*. D 13, 198.

[7] Page, D. N. (1974). Particle emission rates from a black hole. II. Massless particles from a rotating hole. *Phys. Rev*. D 14, 3260.

[8] Unruh W. G. (1976). Absorption cross section of small black holes. *Phys. Rev*. D 14, 3251.

[9] Harmark, T., Natario, J., & Schiappa, R. (2010). Greybody factors for d-dimensional black holes. *Adv. Theor. Math. Phys*. 14, 727-794.

[10] Gonzalez, P., Papantonopoulos, E., & Saavedra, J. (2010). Chern-Simons black holes: scalar perturbations, mass and area spectrum and greybody factors. *Journal of High Energy Phys*. 050.

[11] Kanti, P., Pappas, T., & Pappas, N. (2014). Greybody factors for scalar fields emitted by a higher- dimensional Schwarzschild-de Sitter black hole. *Phys. Rev*. D 90, 124077.

[12] Birmingham, D. B., Sachs, I., & Sen, S. (1997). Three-dimensional black holes and string theory. *Lett*. B 413, 281.

[13] Chan, K. C. K., & Mann, R. B. (1994). Static charged black holes in (2+1) -dimensional dilaton gravity. *Phys. Rev*. D 50, 6385.

[14] Fernando, S. (2005). Greybody factors of charged dilaton black boles in 2+1 dimensions. *Gen. Relativ. Gravit*. 37, 461-481.

[15] Brown, J. D., & York, J. W. (1993). Quasilocal energy and conserved charges derived from the gravitational action. *Phys. Rev*. D 47, 1407-1419.

[16] Wald, R. M. (1984). *General Relativity*. The University of Chicago Press. Chicago and London.

[17] Abramowitz, M., & Stegun, I. A. (1965). *Handbook of Mathematical Functions*. Dover. New York.

[18] Sakalli, I. (2015). Quantization of rotating linear dilaton black holes. *Eur. Phys.* J. C 75, 144.

[19] Olver, F. W. J., Lozier, D. W., Boisvert, R. F., & Clark, C. W. (2010). NIST *Handbook of Mathematical Functions*. Cambridge University Press. New York.

[20] Sakalli, I., & Aslan, O. A. (2016). Absorption cross-section and decay rate of rotating linear dilaton black holes. *Astropar. Phys.* 74, 73-78.

[21] Harmark, T., Natario, J., & Schiappa, R. (2010). Greybody factors for d-dimensional black holes. *Adv. Theor. Math. Phys.* 14, 727.

[22] Das, S. R., Gibbons, G., & Mathur, S. D. (1997). Universality of low energy absorption cross sections for black holes. *Phys. Rev. Lett.* 78,417.

[23] Myers, R. C., & Perry, M. J. (1986). Black holes in higher dimensional space-times. *Ann. Phys.* 172, 304-347.